

Article

Estimates of the Change in the Oceanic Precipitation Off the Coast of Europe due to Increasing Greenhouse Gas Emissions

Francisco J. Tapiador ^{1,*} , Andrés Navarro ¹ , Cecilia Marcos ²  and Raúl Moreno ¹ 

¹ Earth and Space Sciences Group (ESS), Institute of Environmental Sciences (ICAM), University of Castilla-La Mancha (UCLM), 45071 Toledo, Spain; Andres.Navarro@uclm.es (A.N.); raul.moreno@uclm.es (R.M.)

² National Meteorology Agency (AEMET), 28071 Madrid, Spain; cmarcosm@aemet.es

* Correspondence: Francisco.Tapiador@uclm.es; Tel.: +34-925-268-800 (ext. 5762)

Received: 28 June 2018; Accepted: 25 July 2018; Published: 31 July 2018



Abstract: This paper presents a consensus estimate of the changes in oceanic precipitation off the coast of Europe under increasing greenhouse gas emissions. An ensemble of regional climate models (RCMs) and three gauge and satellite-derived observational precipitation datasets are compared. While the fit between the RCMs' simulation of current climate and the observations shows the consistency of the future-climate projections, uncertainties in both the models and the measurements need to be considered to generate a consensus estimate of the potential changes. Since oceanic precipitation is one of the factors affecting the thermohaline circulation, the feedback mechanisms of the changes in the net influx of freshwater from precipitation are relevant not only for improving oceanic-atmospheric coupled models but also to ascertain the climate signal in a global warming scenario.

Keywords: precipitation; satellites; climate models; regional climate models

1. Introduction

The importance of a precise estimation of oceanic precipitation derives from the freshening effect exerted on the oceanic surface. In certain high European latitudes of the Atlantic Ocean, precipitation exceed evaporation, so precipitation acts as a net source of freshwater that decreases the salinity and thus the density of surface waters. It has been known for some time that the extent in which dense, salty water sinks in the North Atlantic largely affect this circulation [1]. This freshening is one of the processes that has been proposed [2,3] to explain the observed slowing down of the Atlantic meridional overturning circulation in middle latitudes [4].

The precise measurement of such process has been addressed by several authors [5–7]. For instance, Meier has provided insight into future changes in the salinity of the Baltic Sea [6,8] while pointing out that salinity projections have suffered from the large uncertainties of precipitation estimates coming from models [6]. There is certainly agreement in that to address model shortcomings and provide a more precise quantification of the oceanic precipitation, both satellite estimates of precipitation and global circulation/climate models (GCMs) are required.

GCMs are instrumental for improving our understanding of the climate, but their coarse horizontal grid spacing (typically 50–300 km) smooths the highly variable field of precipitation [9]. On the other hand, regional climate models (RCMs) have been proved useful to provide fine-scale, physically-based downscaling [10–12] of global models' outputs. The idea behind an RCM is to improve the simulations by nesting the model on a GCM [13–15]. RCMs have been used to analyze processes (such as

orographic enhancement) that GCMs are unable to adequately resolve [9,16,17]. However, criticisms of RCMs remain.

In order to ascertain how reliable an RCM's projection is, present-climate simulations are compared with observed climatologies. If the RCM compares favorably, then it is assumed that the model is suitable to make projections of the future climate. Indeed, this is a necessary, but by no means sufficient, condition.

Several studies have compared RCM simulations with observed climatologies [13,18–20] focusing on changes in mean seasonal values and interannual variability [14,21], including such data for precipitation [22,23]. In these particular cases, comparisons for present or future climate [24] are often done against CRU (climatic research unit) data [25,26]. The CRU dataset, however, is limited to land areas. Moreover, given the differences between oceanic and land precipitation [27] and the dissimilar surface feedbacks between the two cases [28], a separate validation should be required to analyze the uncertainties in future land and oceanic precipitation. Therefore, satellite observations of oceanic precipitation are needed, but this limits comparisons to the 39 years from 1979 to the present. The most reliable estimates of oceanic precipitation require microwave instrumentation, further reducing the comparison window from 1987 at best. On the other hand, PRUDENCE RCM simulations cover a specific interval (1960–1990; cf. Section 2.2 below for the reason of such specific dates), so the comparison has to be limited to the satellite-models overlapping period. This is not optimum, since the observational data includes infrared (IR) estimates which are known to be indirect, but it is a required compromise.

2. Materials and Methods

2.1. Observations

GPCP, CMAP and CPC PREC data (CPC hereafter) were used as the observational databases to determine the current climate precipitation climatology baseline. Table 1 shows a comparison of the features of the empirical datasets. Subsections below briefly describe relevant information for each product.

Table 1. Summary of the empirical base.

Dataset	Temporal Resolution	Spatial Aggregation	Geographical Coverage	Original Sources	Period Covered
<i>Observations</i>					
CPC	Monthly	$2.5^\circ \times 2.5^\circ$	Global	Raingauge + EOFs	1948–present
CMAP	Monthly	$2.5^\circ \times 2.5^\circ$	Global	Satellite + Raingauge	1979–present
GPCP ¹	Daily	$2.5^\circ \times 2.5^\circ$	Global	Satellite + Raingauge	1979–present
<i>Simulations</i>					
PRUDENCE	Daily	$0.5^\circ \times 0.5^\circ$	Europe	RCMs	1960–1990 2070–2100 (A2)

¹ $1.0^\circ \times 1.0^\circ$ data available for 1996–2015.

2.1.1. CPC PREC Data

The Climate Prediction Center (CPC) disseminates a product named as NOAA's Precipitation Reconstruction Dataset (PREC) at a $0.5^\circ \times 0.5^\circ$ spatial resolution ([29], hereafter CPC data). Original data come from rain gauge observations from over 17,000 stations from the Global Historical Climatology Network (GHCN) version 2 and the Climate Anomaly Monitoring System (CAMS) datasets. Interpolation is performed using Gandin's optimal interpolation (OI) technique [30]. The ocean part of the dataset is calculated using an empirical orthogonal function (EOF) reconstruction of historical observations over ocean. The EOF modes are derived from EOF analysis of the satellite estimates for later years (1979–1998) with complete spatial coverage. The current version, 1.0, is based

on the first 8 EOF global modes for each of the four seasons and the first four EOF modes of the residual components of the eight EOF global modes over Atlantic Ocean areas [29].

2.1.2. CMAP Data

The US Climate Prediction Center's Merged Analysis of Precipitation (CMAP) has made available monthly land and ocean estimates of global precipitation in which observations from rain gauges are merged with satellite precipitation estimates. The spatial resolution of the dataset is $2.5^\circ \times 2.5^\circ$ for the 1979–2018 period. The merging technique is fully described in [31]. As stated in the CMAP dataset documentation, the methodology first reduces random errors by linearly combining satellite estimates using a maximum likelihood method that gives an inversely proportional weight to the linear combination coefficients in relation to the square of the random error of the individual sources. Over global land areas, the random error is defined for each time period and grid location by comparing the data source with the rain gauge analysis over the surrounding area. Over oceans, the random error is defined by comparing the data sources with the rain gauge observations over the Pacific atolls. Bias is reduced by blending the data sources in the second step using the variational blending technique of Reynolds [32]. The actual CMAP precipitation data version used in this study was provided by the NOAA/OAR/ESRL PSD.

2.1.3. GPCP Data

The International Global Precipitation Climatology Project (GPCP) has produced a comprehensive, mixed rain gauge and satellite global precipitation product for both land and ocean. Several papers [33–37] describe the GPCP product at $2.5^\circ \times 2.5^\circ$ monthly resolution. This resolution is improved to $1.0^\circ \times 1.0^\circ$ daily estimates for the period 1996–2015 (and expected to be continued till present for the near future). Data sources includes the FAO, CRU, GHCN and the additional GPCC original sources seen above. Both land and ocean areas are covered thanks to the use of geo-stationary and low earth orbit satellites, including visible (VIS), infrared (IR) and passive microwave (PMW) sensors.

Satellite information is used to cover the gaps in the rain gauge data, with a physically-based algorithm being used for the retrieval of surface rain from PMW sensors and a statistically-based relationship based on cloud top temperature for VIS and IR data. Screening procedures and separate treatment of outliers ensures the homogeneity of the time series. Only the homogenized and nearly gap-free time series of 9343 stations are taken into account, but the long-term means of over 28,000 stations are used in order to estimate average precipitation fields [38]. All interpolations are performed using ordinary kriging with local and seasonal decorrelation lengths estimated from the observations [38].

2.2. RCMs Simulations

Eight RCMs were used to compare present-climate and increased greenhouse gases scenario simulations. These RCMs were part of the Prediction of Regional Scenarios and Uncertainties for Defining European Climate Change Risks and Effects (PRUDENCE) project, which aimed to provide high-resolution future scenarios of climate change for Europe [39]. The models are the DMI's HIRHAM [40], ETH's CHRM [41], KNMI's RACMO [42], GKSS's CLM [43], Hadley Center's HadRM3H [44], MPI's REMO [45], UCLM's PROMES [46] and the SMHI's RCAO [47–49].

Full 30-year simulations were computed for nominal present (1960–1990) and future (2070–2100) SRES-A2 scenario climates. The present-climate period was selected following WMO's technical regulations, who recognizing the need for a stable base for long-term climate change and variability assessment, fixed a reference, 30-year period from 1 January 1961 to 31 December 1990. This period is used to compare climate change and variability across all countries relative to this standard reference period.

The eight RCM models were forced with the HadAM3H-GCM model [50]. Initial fields of sea surface temperature, sulfate aerosols and other forcings were taken from the GCM to initialize the

RCMs. Greenhouse gases concentrations forcings were obtained from the IPCC [51] for the A2 scenario. The GCM drove the RCMs every 6 h on the corresponding domain contours (typically 8 to 10 points) with perfect boundary conditions.

Current-climate simulation used observed sea surface temperatures (SSTs) from the HadISST database [52], while future period values were obtained from the HadCM3 coupled atmosphere ocean global climate model [53]. More precisely, future monthly SST anomalies were obtained adding present-climate SST to present-climate SST anomalies, as described in [54].

The different domains of the individual RCMs cover most of Europe, the European shore of the Atlantic, the Mediterranean, and Northern Africa. There is a common region covering the center and south of Europe. To make our results fully comparable, this overlapping region was selected as our study area.

Daily precipitation values from the observational datasets were interpolated to a common $0.5^\circ \times 0.5^\circ$ grid by bilinear interpolation, and monthly means were obtained for each cell. The results of the simulations were also interpolated to a common grid of 0.5° resolution (roughly 50 km for these latitudes). The first year of each simulation (either 1960 or 2070) was used as spin-up period to allow the RCMs to adjust their large-scale conditions, especially those related with soil moisture conditions.

In order to have a common period for both observations and RCMs simulations, mean climatological values of the 10-years overlapping period of the datasets were used. Although a full climatological characterization would require a 30-year period, shorter periods have been found useful in similar studies [51]. For future climate, the values from January 2089 to January 2099 were used, thus allowing both datasets to be at the same distance from their corresponding spinning periods.

The reason for using the PRUDENCE data instead of more recent datasets is twofold. First, the dataset has withstood time and proved its validity over the years, with a large number of publications analyzing and validating the results. The dataset has been independently cross-validated over a long period of time and no major issues have arisen. More recent datasets, such as CORDEX, still have to pass the test of time. Secondly, the RCMs were nested on a GCM and not in reanalysis which, in a sense, makes the comparison between present and future climates more consistent (since by definition there is no reanalysis of the future).

Also, while the use of SRES scenarios instead of representative concentration pathways (RCP) may seem outdated in 2018, PRUDENCE results are still used to inform policies for climate change adaptation, and therefore it is still worth to examine how they compare with observations.

2.3. Averaging Method

The model data can be thought as a four-dimensional hypercube of longitude, latitude, time and model. Thus, we note

$$PR_{ijkm} \quad (1)$$

for the estimate of precipitation of the m -eth RCM for the k -eth month, at j -eth latitude and i -eth longitude. Averaging over the k index for all the n months gives the average of the model:

$$\text{Average of the model } m = \frac{1}{n} \sum_{k=1}^{k=12} PR_{ijkm} \equiv \overline{PR_{ijm}}^k \quad (2)$$

where the overbar denotes the average over k . Further averaging over all the RCMs ($m = 10$) yields the average of the ensemble:

$$\text{Average of the RCM ensemble} = \frac{1}{10 \cdot n} \sum_{m=1}^{m=10} \sum_{k=1}^{k=12} PR_{ijkm} \equiv \overline{\overline{PR_{ij}}^k}^m \equiv \langle RCM \rangle. \quad (3)$$

The ensemble mean $\langle \text{RCM} \rangle$ is thus a two-dimension field ($i \times j$). The same averaging procedure is performed with the observational datasets. Thus, for instance for the GPCP:

$$\text{GPCP Average} = \frac{1}{n} \sum_{k=\text{time}_1}^{k=\text{time}_n} PR_{ijk(\text{GPCP})} \equiv \overline{PR_{ij(\text{GPCP})}^k} \equiv \text{GPCP}. \quad (4)$$

The precipitation average of this observational dataset is noted just as “GPCP” in order to keep the notation as clean as possible. The same for CPC and CMAP.

3. Results

Figure 1 shows the mean precipitation estimates for the model ensemble mean $\langle \text{RCMs} \rangle$ and the three observational databases. The agreement of present climate conditions is noticeable albeit differences exist, for instance, in the North Sea and the Adriatic Sea. Table 2 gives a quantitative overview of the cross-correlations between the RCMs, the ensemble mean, and the observations. The $\langle \text{RCMs} \rangle$ compares well with the data being the best correlation with the GPCP (0.842; compared to 0.822 for the CPC, and to 0.792 for the CMAP datasets).

The correlations for present climate are high enough to confirm the relatively good performances of the RCMs and to have confidence in their projections for future climates.

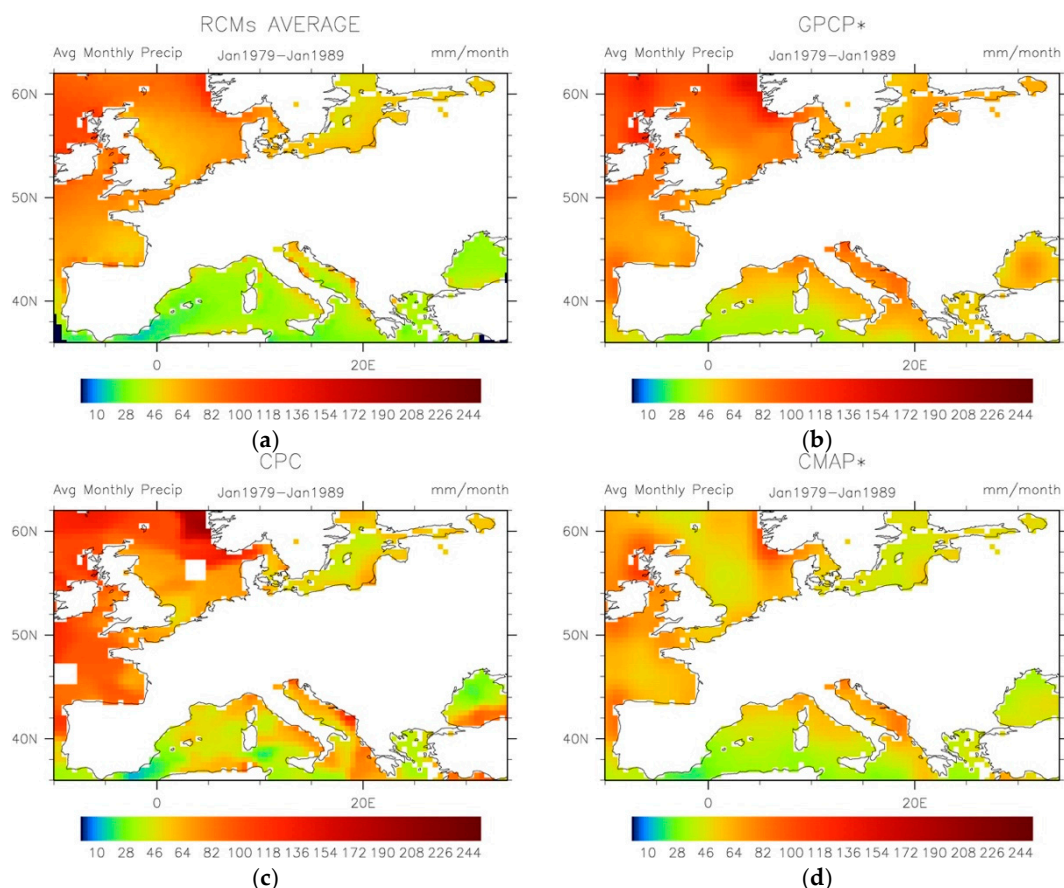


Figure 1. Observational estimates of the mean precipitation for the January 1979–January 1989 period. Units are in mm/month. (a) RCM average; (b) GPCP estimate; (c) CPC estimate; (d) CMAP estimate.

An important variable of interest to evaluate the changes in oceanic precipitation is the precipitation climate signal, which is the difference between the precipitation in the future and at present. Such reference precipitation at present can be either the RCM outputs or the observational

datasets. Figure 2 shows the climate signal for the ensemble mean in future climate $\langle \text{RCMs} \rangle_{\text{FC}}$ minus the ensemble mean of the RCMs at present $\langle \text{RCMs} \rangle_{\text{PC}}$. The figure also shows the climate signal taken separately with reference from the three observational datasets, GPCP, CMAP and CPC.

The differences between $\langle \text{RCMs} \rangle_{\text{FC}}$ and $\langle \text{RCMs} \rangle_{\text{PC}}$ are smaller than those between $\langle \text{RCMs} \rangle_{\text{FC}}$ and the observations. Amongst them all, the CMAP-based climate signal exhibits the largest projected increases in oceanic precipitation with more than a 50% difference above 56° N.

Table 2. Cross-correlations (R) of the monthly mean present-climate precipitation (January 1979–January 1989) for the three observational datasets (CPC, GPCP and CMAP), the eight individual RCMs, and the RCMs ensemble average ($\langle \text{RCMs} \rangle$).

	CPC ¹	GPCP ¹	CMAP ¹	HIR.	CHRM	RCAO	CLM	Had.	REMO	PRO.	RAC.	$\langle \text{RCMs} \rangle$
					<i>Ocean</i>	<i>Only</i>						
CPC ¹	1	0.866	0.808	0.775	0.8	0.645	0.836	0.625	0.743	0.804	0.667	0.822
GPCP ¹		1	0.885	0.788	0.768	0.731	0.832	0.658	0.748	0.741	0.745	0.842
CMAP ¹			1	0.786	0.715	0.634	0.824	0.583	0.701	0.741	0.683	0.792
HIRHAM				1	0.807	0.701	0.848	0.755	0.726	0.798	0.77	0.895
CHRM					1	0.749	0.871	0.728	0.859	0.792	0.77	0.919
RCAO						1	0.725	0.742	0.822	0.655	0.918	0.889
CLM							1	0.685	0.783	0.808	0.772	0.907
HadRM3H								1	0.717	0.704	0.782	0.854
REMO									1	0.742	0.775	0.902
PROMES										1	0.719	0.863
RACMO											1	0.914
$\langle \text{RCMs} \rangle$												1

¹ Distance-weighted resampled at 0.5° × 0.5° resolution from the original 2.5° × 2.5° data.

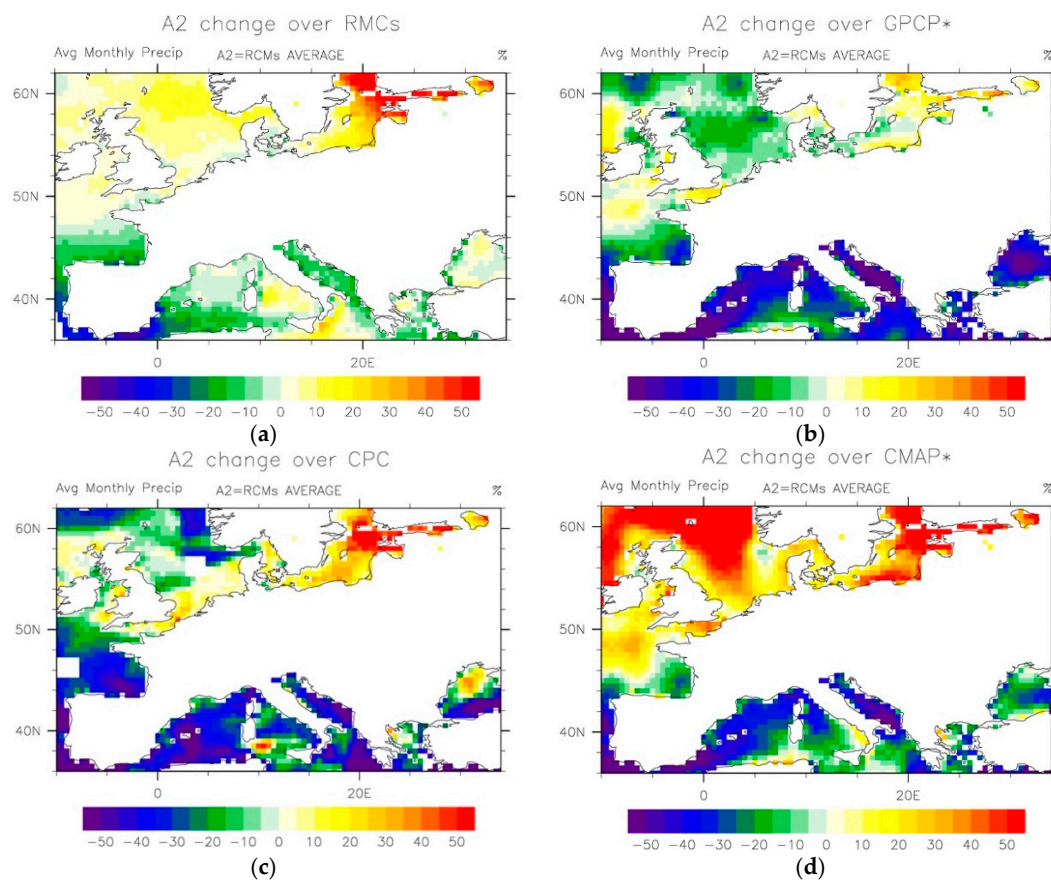


Figure 2. Differences in oceanic precipitation for the A2 scenario (a) taking the RCMs as reference for present climate; (b) taking GPCP as reference; (c) taking CPC as reference; and (d) taking CMAP as reference. Units are percentage over present-climate precipitation in the RCMs.

Since the GPCP is the dataset that presents the best fit with present-climate simulations ($0.842 R^2$; Table 2), differences with respect to GPCP in the future can be interpreted as the best-case scenario. That is, uncertainties in the climate signal when GPCP is used as the reference are the minimum uncertainties to be found.

Figure 3 shows the distribution of the differences between future- and present-climate when either the average of the RCMs (x-axis) or the GPCP (y-axis) are used as the present-climate climatology. Data in the upper-left and the lower-right quadrants are those in which the precipitation climate signal differs in both reference datasets. In the other two quadrants (1st: upper-right, and 3rd: lower-left), there is a consensus in the sign of the climate signal: positive in the case of the 1st quadrant and negative for the 3rd.

The instances in which the climate signal is negative (less precipitation expected in the future) if the reference data is the RCMs average but positive if the reference data is the GPCP (i.e., upper-left, 2nd quadrant) are limited. However, there is large number of cases for which the climate signal is positive in the first case and negative in the second (lower-right: 4th quadrant); that is, there are many places where the models predict more precipitation in the future when their simulations are compared with their own present-climate simulations, but less when compared with the GPCP reference for present-climate. Indeed, Figure visually represents the underlying reason, model bias, while at the same time providing a succinct account of the consensus in the climate signal between models and observations (GPCP here).

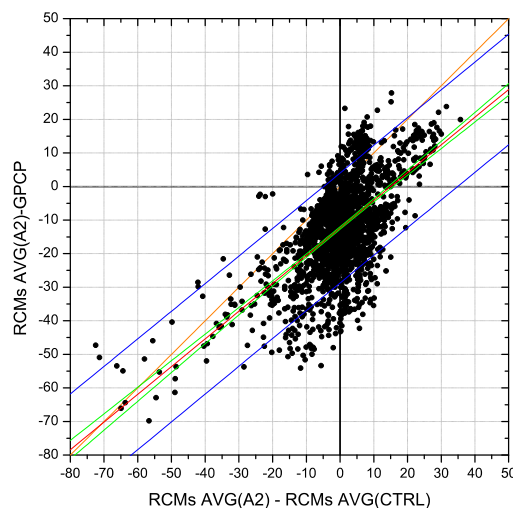


Figure 3. Comparison of the differences in the estimated changes in the mean precipitation of Europe in the A2 scenario between either using the GPCP as reference or the RCMs average for present-climate conditions (control run; CTRL). Lines are the perfect match (orange line), the best linear fit (red line), the 85% confidence interval of the best linear fit (green lines) and the 85% prediction limits (blue lines). Each dot in the plots represent the monthly average for a model grid point. Dots in the 2nd quadrant (upper-left) and in the 4th quadrant (bottom-right) indicate locations in which the reference dataset shows a discrepancy in the precipitation climate signal. Notice that since the plot compares differences, the RCMs AVG (A2) can feature in both axes. Each dot represents the value of the 30-year averages for that grid point (i.e., $\overline{PR_{ij}^k}^m$).

Therefore, a metric for the consensus in the precipitation climate signal between the RCMs and the references (GPCP, CMAP and CPC) can be built by the segmentation of the grid points into four quadrants. The resulting three categories (Figure 4): consensus (1st and 3rd quadrants), positive-negative dissent (2nd quadrant), and negative-positive dissent (4th quadrant) are helpful to evaluate the changes depicted in Figure 2. Where consensus exists, the changes can be considered more robust while if there is dissent then the model bias may be obscuring the signal.

Figure 4 shows that the RCMs and observations agree in most of the area of interest. Nevertheless, discrepancies appear in the Black Sea, the seas south of Italy, the North Sea above 56° North and, of opposite sign, off North Spain and in the English Channel. If we deem GPCP as the most reliable dataset for reference (Figure 4a), discrepancies are mainly restricted to positive bias in the North Sea, the seas south of Italy and the Black Sea. Conversely, CPC and CMAP (Figure 4b,c) show larger consensus areas than those with the GPCP reference, especially in the North Sea, but differences in the amount of precipitation change are higher than those of RCMs and GPCP (cf. Figure 2).

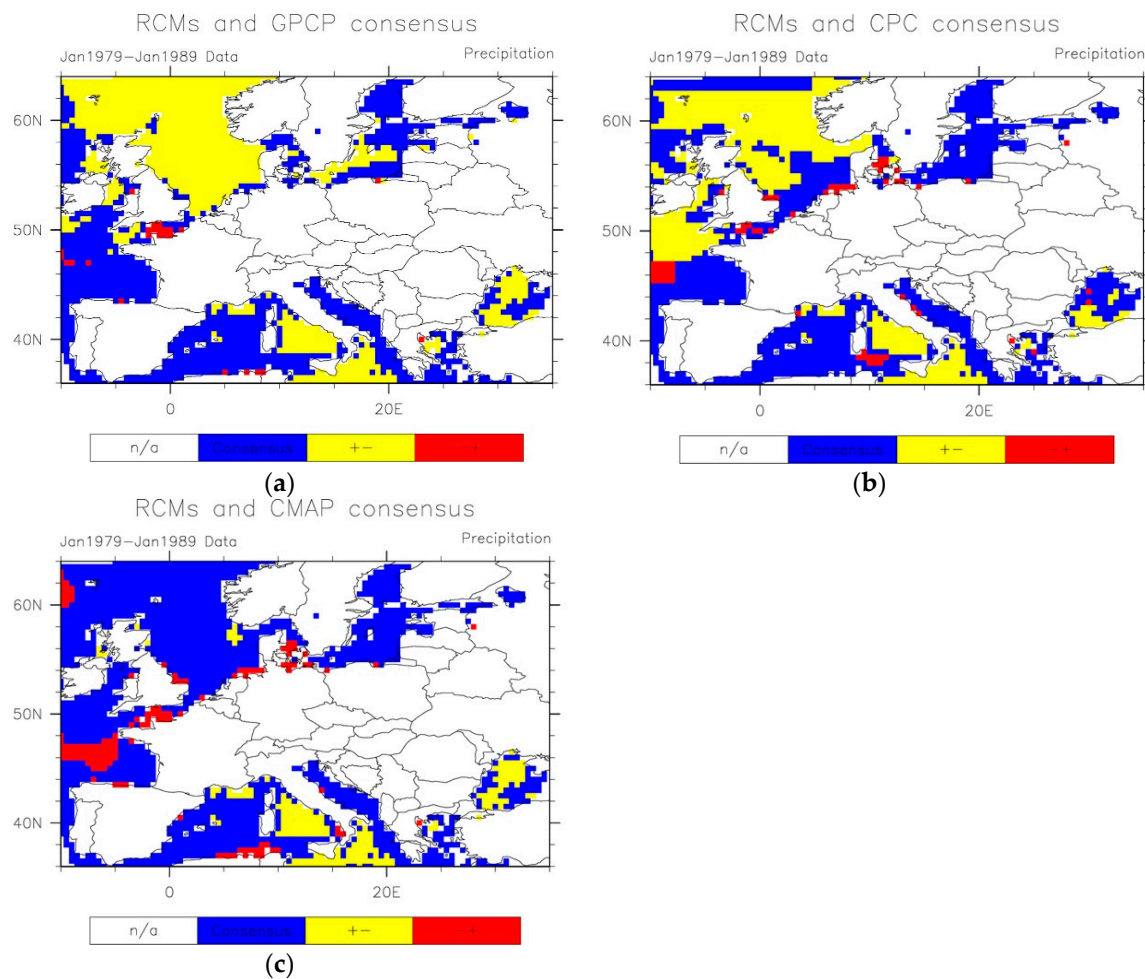


Figure 4. Consensus/dissent for the January 1979–January 1989 mean precipitation between RCMs and GPCP (a); RCMs and CPC (b); and RCMs and CMAP (c). Blues represent consensus between RCMs and observational datasets (1st and 3rd quadrants in Figure 3); yellows dissent (places where the models predict more precipitation in the future if they are compared with the present-climate, model derived reference but less if compared with present-climate GPCP reference, 4th quadrant); and reds those cases for which the climate signal is negative (less precipitation in the future) if the reference data is the RCMs average for present climate, but positive if the reference data is the GPCP (upper-left, 2nd quadrant).

If we take a closer look at Figures 2 and 4, precipitation is expected to decrease with high confidence (i.e., large consensus) in the Mediterranean Basin—the Western Mediterranean Sea, the Adriatic Sea and the Aegean Sea, in the Bay of Biscay, and in the Kattegat Sea area. In those areas, the freshening effect of precipitation is expected to be reduced in the A2 emissions scenario, yielding an increase in salinity. However, a net increase is expected in the Celtic Sea and in the Baltic

Sea. The analysis of the North Sea is more complex because of the disagreement between GPCP and RCMs (Figure 4a). Nevertheless, when compared with CMAP (Figure 4c) a net increase in precipitation is observed.

4. Conclusions

In this paper, the oceanic precipitation projections of eight RCMs for the present-climate and the A2-SRES future-climate scenario have been compared with satellite and offshore gauge estimates. Notwithstanding observational errors [55,56] and several other uncertainties, the results show that the RCMs consistently reproduce observed oceanic precipitation of Europe, thus increasing the confidence in such models being capable of estimating changes in the future oceanic precipitation patterns.

By integrating the uncertainties in both the observational and the modeled oceanic precipitation, a consensus estimate is made, resulting in increased confidence of an overall net increase of the freshening above 46° North and a relative decrease in the Mediterranean Basin.

Since oceanic precipitation is one of the factors affecting the thermohaline circulation, the feedback mechanisms of the changes in the net influx of freshwater from precipitation are relevant not only for improving oceanic-atmospheric coupled models but also to ascertain the climate signal in a global warming scenario. Within this context, the use of satellite-derived datasets is crucial as they are the only available means to build the reference datasets required to estimate the magnitude of the changes and their uncertainties. Also, new modeling initiatives such as the Coordinated Regional Climate Downscaling Experiment (CORDEX) are proving to be instrumental to ascertain the effects of precipitation in the global hydrological cycle [57–63], and especially about its impacts in Europe (EURO-CORDEX [64]).

Author Contributions: F.J.T. led the research and outlined the draft of the manuscript. A.N., C.M., and R.M. contributed to analysis, plotting, and manuscript writing.

Funding: This research was funded by the Ministerio de Economía y Competitividad, Ciencia e Innovación under grant numbers CGL2013-48367-P, CGL2016-80609-R, and by the Ministerio de Educación under FPU grant 13/02798.

Acknowledgments: Thanks are due to Nabhonil Kar (Princeton University) for his editing of the manuscript.

Conflicts of Interest: The authors declare no conflicts of interest.

References

- Hartmann, D.L. *Global Physical Climatology*, 2nd ed.; Elsevier: Cambridge, MA, USA, 2016.
- Dickson, B.; Yashayaev, I.; Meincke, J.; Turrell, B.; Dye, S.; Holfort, J. Rapid freshening of the deep North Atlantic Ocean over the past four decades. *Nature* **2002**, *416*, 832–837. [[CrossRef](#)] [[PubMed](#)]
- Dickson, R.; Rudels, B.; Dye, S.; Karcher, M.; Meincke, J.; Yashayaev, I. Current estimates of freshwater flux through Arctic and subarctic seas. *Prog. Oceanogr.* **2007**, *73*, 210–230. [[CrossRef](#)]
- Cunningham, S.A.; Kanzow, T.; Rayner, D.; Baringer, M.O.; Johns, W.E.; Marotzke, J.; Longworth, H.R.; Grant, E.M.; Hirschi, J.J.-M.; Beal, L.M.; et al. Temporal variability of the Atlantic meridional overturning circulation at 26.5°N. *Science* **2007**, *317*, 935–938. [[CrossRef](#)] [[PubMed](#)]
- Brossier, C.L.; Béranger, K.; Drobinski, P. Ocean response to strong precipitation events in the Gulf of Lions (northwestern Mediterranean Sea): A sensitivity study. *Ocean Dyn.* **2012**, *62*, 213–226. [[CrossRef](#)]
- Meier, H.E.M.; Kjellström, E.; Graham, L.P. Estimating uncertainties of projected Baltic Sea salinity in the late 21st century. *Geophys. Res. Lett.* **2006**, *33*. [[CrossRef](#)]
- Zeng, L.; Chassignet, E.P.; Schmitt, R.W.; Xu, X.; Wang, D. Salinification in the South China Sea Since Late 2012: A Reversal of the Freshening Since the 1990s. *Geophys. Res. Lett.* **2018**, *45*, 2744–2751. [[CrossRef](#)]
- Meier, H.E.M. Baltic Sea climate in the late twenty-first century: A dynamical downscaling approach using two global models and two emission scenarios. *Clim. Dyn.* **2006**, *27*, 39–68. [[CrossRef](#)]
- Pan, X.; Li, X.; Cheng, G.; Hong, Y. Effects of 4D-Var data assimilation using remote sensing precipitation products in a WRF model over the complex terrain of an arid region river basin. *Remote Sens.* **2017**, *9*, 963. [[CrossRef](#)]

10. Feser, F.; Rockel, B.; von Storch, H.; Winterfeldt, J.; Zahn, M. Regional Climate Models Add Value to Global Model Data: A Review and Selected Examples. *Bull. Am. Meteorol. Soc.* **2011**, *92*, 1181–1192. [[CrossRef](#)]
11. Giorgi, F.; Marinucci, M.R.; Visconti, G. A 2XCO₂ climate change scenario over Europe generated using a limited area model nested in a general circulation model 2. Climate change scenario. *J. Geophys. Res. Atmos.* **1992**, *97*, 10011–10028. [[CrossRef](#)]
12. Kendon, E.J.; Jones, R.G.; Kjellström, E.; Murphy, J.M. Using and designing GCM-RCM ensemble regional climate projections. *J. Clim.* **2010**, *23*, 6485–6503. [[CrossRef](#)]
13. Giorgi, F.; Bi, X.; Pal, J.S. Mean, interannual variability and trends in a regional climate change experiment over Europe. I. Present-day climate (1961–1990). *Clim. Dyn.* **2004**, *22*, 733–756. [[CrossRef](#)]
14. Giorgi, F.; Bi, X.; Pal, J. Mean, interannual variability and trends in a regional climate change experiment over Europe. II: Climate change scenarios (2071–2100). *Clim. Dyn.* **2004**, *23*, 839–858. [[CrossRef](#)]
15. Robertson, A.W.; Qian, J.-H.; Tippett, M.K.; Moron, V.; Lucero, A. Downscaling of Seasonal Rainfall over the Philippines: Dynamical versus Statistical Approaches. *Mon. Weather Rev.* **2012**, *140*, 1204–1218. [[CrossRef](#)]
16. Choi, H., II. Application of a land surface model using remote sensing data for high resolution simulations of terrestrial processes. *Remote Sens.* **2013**, *5*, 6838–6856. [[CrossRef](#)]
17. Zhang, M.; Luo, G.; De Maeyer, P.; Cai, P.; Kurban, A. Improved atmospheric modelling of the oasis-desert system in central Asia using WRF with actual satellite products. *Remote Sens.* **2017**, *9*, 1273. [[CrossRef](#)]
18. Déqué, M.; Jones, R.G.; Wild, M.; Giorgi, F.; Christensen, J.H.; Hassell, D.C.; Vidale, P.L.; Rockel, B.; Jacob, D.; Kjellström, E.; et al. Global high resolution versus Limited Area Model climate change projections over Europe: Quantifying confidence level from PRUDENCE results. *Clim. Dyn.* **2005**, *25*, 653–670. [[CrossRef](#)]
19. Räisänen, J.; Hansson, U.; Ullerstig, A.; Döscher, R.; Graham, L.P.; Jones, C.; Meier, H.E.M.; Samuelsson, P.; Willén, U. European climate in the late twenty-first century: Regional simulations with two driving global models and two forcing scenarios. *Clim. Dyn.* **2004**, *22*, 13–31. [[CrossRef](#)]
20. Schoetter, R.; Hoffmann, P.; Rechid, D.; Schlünzen, K.H. Evaluation and bias correction of regional climate model results using model evaluation measures. *J. Appl. Meteorol. Climatol.* **2012**, *51*, 1670–1684. [[CrossRef](#)]
21. Déqué, M.; Rowell, D.P.; Lüthi, D.; Giorgi, F.; Christensen, J.H.; Rockel, B.; Jacob, D.; Kjellström, E.; De Castro, M.; Van Den Hurk, B. An intercomparison of regional climate simulations for Europe: Assessing uncertainties in model projections. *Clim. Chang.* **2007**, *81*, 53–70. [[CrossRef](#)]
22. Beniston, M.; Stephenson, D.B.; Christensen, O.B.; Ferro, C.A.T.; Frei, C.; Goyette, S.; Halsnaes, K.; Holt, T.; Jylhä, K.; Koffi, B.; et al. Future extreme events in European climate: An exploration of regional climate model projections. *Clim. Chang.* **2007**, *81*, 71–95. [[CrossRef](#)]
23. Tapiador, F.J.; Sánchez, E.; Gaertner, M.A. Regional changes in precipitation in Europe under an increased greenhouse emissions scenario. *Geophys. Res. Lett.* **2007**, *34*, L06701. [[CrossRef](#)]
24. Pal, J.S.; Giorgi, F.; Bi, X. Consistency of recent European summer precipitation trends and extremes with future regional climate projections. *Geophys. Res. Lett.* **2004**, *31*. [[CrossRef](#)]
25. New, M.; Lister, D.; Hulme, M.; Makin, I. A high-resolution data set of surface climate over global land areas. *Clim. Res.* **2002**, *21*, 1–25. [[CrossRef](#)]
26. Harris, I.; Jones, P.D.D.; Osborn, T.J.J.; Lister, D.H.H. Updated high-resolution grids of monthly climatic observations—the CRU TS3.10 Dataset. *Int. J. Climatol.* **2014**, *34*, 623–642. [[CrossRef](#)]
27. Doherty, R.M.; Hulme, M.; Jones, C.G. A gridded reconstruction of land and ocean precipitation for the extended tropics from 1974 to 1994. *Int. J. Climatol.* **1999**, *19*, 119–142. [[CrossRef](#)]
28. Koster, R.D.; Suarez, M.J. Relative contributions of land and ocean processes to precipitation variability. *J. Geophys. Res.* **1995**, *100*, 13775. [[CrossRef](#)]
29. Chen, M.; Xie, P.; Janowiak, J.E.; Arkin, P.A.; Chen, M.; Xie, P.; Janowiak, J.E.; Arkin, P.A. Global Land Precipitation: A 50-yr Monthly Analysis Based on Gauge Observations. *J. Hydrometeorol.* **2002**, *3*, 249–266. [[CrossRef](#)]
30. Reynolds, R.W.; Smith, T.M. Improved global sea surface temperature analyses using optimum interpolation. *J. Clim.* **1994**, *7*, 929–948. [[CrossRef](#)]
31. Xie, P.; Arkin, P.A. Global precipitation: A 17-year monthly analysis based on gauge observations, satellite estimates and numerical model outputs. *Bull. Am. Meteorol. Soc.* **1997**, *78*, 2539–2558. [[CrossRef](#)]
32. Reynolds, R.W. A Real-Time Global Sea Surface Temperature Analysis. *J. Clim.* **1988**, *1*, 75–87. [[CrossRef](#)]

33. Huffman, G.J.; Adler, R.F.; Rudolf, B.; Schneider, U.; Keehn, P.R. Global precipitation estimates based on a technique for combining satellite-based estimates, rain gauge analysis, and NWP model precipitation information. *J. Clim.* **1995**, *8*, 1284–1295. [[CrossRef](#)]
34. Huffman, G.J.; Adler, R.F.; Arkin, P.; Chang, A.; Ferraro, R.; Gruber, A.; Janowiak, J.; McNab, A.; Rudolf, B.; Schneider, U. The Global Precipitation Climatology Project (GPCP) Combined Precipitation Dataset. *Bull. Am. Meteorol. Soc.* **1997**, *78*, 5–20. [[CrossRef](#)]
35. Huffman, G.J.; Adler, R.F.; Morrissey, M.M.; Bolvin, D.T.; Curtis, S.; Joyce, R.; McGavock, B.; Susskind, J. Global Precipitation at One-Degree Daily Resolution from Multisatellite Observations. *J. Hydrometeorol.* **2001**, *2*, 36–50. [[CrossRef](#)]
36. Huffman, G.J.; Adler, R.F.; Bolvin, D.T.; Gu, G. Improving the global precipitation record: GPCP Version 2.1. *Geophys. Res. Lett.* **2009**, *36*, L17808. [[CrossRef](#)]
37. Adler, R.F.; Sapiiano, M.R.P.; Huffman, G.J.; Wang, J.J.; Gu, G.; Bolvin, D.; Chiu, L.; Schneider, U.; Becker, A.; Nelkin, E.; et al. The Global Precipitation Climatology Project (GPCP) monthly analysis (New Version 2.3) and a review of 2017 global precipitation. *Atmosphere* **2018**, *9*, 138. [[CrossRef](#)] [[PubMed](#)]
38. Smith, T.M.; Yin, X.; Gruber, A. Variations in annual global precipitation (1979–2004), based on the Global Precipitation Climatology Project 2.5° analysis. *Geophys. Res. Lett.* **2006**, *33*. [[CrossRef](#)]
39. Christensen, J.H.; Christensen, O.B. A summary of the PRUDENCE model projections of changes in European climate by the end of this century. *Clim. Chang.* **2007**, *81*, 7–30. [[CrossRef](#)]
40. Christensen, J.H.; Christensen, O.B.; Lopez, P.; van Meijgaard, E.; Botzet, M. The HIRHAM 4 regional atmospheric climate model 1996.
41. Vidale, P.L. Predictability and uncertainty in a regional climate model. *J. Geophys. Res.* **2003**, *108*, 4586. [[CrossRef](#)]
42. Lenderink, G.; Hurk, B.; Meijgaard, E.; Ulden, A.; Cuijpers, H. Simulation of Present-Day Climate in RACMO2: First Results and Model Developments. 2003. Available online: <http://bibliotheek.knmi.nl/knmipubTR/TR252.pdf> (accessed on 28 June 2018).
43. Steppeler, J.; Doms, G.; Schättler, U.; Bitzer, H.W.; Gassmann, A.; Damrath, U.; Gregoric, G. Meso-gamma scale forecasts using the nonhydrostatic model LM. *Meteorol. Atmos. Phys.* **2003**, *82*, 75–96. [[CrossRef](#)]
44. Buonomo, E.; Jones, R.; Huntingford, C.; Hannaford, J. On the robustness of changes in extreme precipitation over Europe from two high resolution climate change simulations. *Q. J. R. Meteorol. Soc.* **2007**, *133*, 65–81. [[CrossRef](#)]
45. Jacob, D. The role of water vapour in the atmosphere. A short overview from a climate modeller's point of view. *Phys. Chem. Earth Part A Solid Earth Geod.* **2001**, *26*, 523–527. [[CrossRef](#)]
46. Castro, M.; Fernandez, C.; Gaertner, M.A. Description of a mesoscale atmospheric numerical model. In *Mathematics, Climate and Environment*; Diaz, J.I., Lions, J., Eds.; Masson: Paris, France, 1993; pp. 230–253.
47. Döscher, R.; Willén, U.; Jones, C.; Rutgersson, A.; Meier, H.E.M.; Hansson, U.; Graham, L.P. The development of the regional coupled ocean-atmosphere model RCAO. *Boreal Environ. Res.* **2002**, *7*, 183–192.
48. Jones, C.; Carvalho, L.M.V.; Higgins, R.W.; Waliser, D.E.; Schemm, J.K.E. A statistical forecast model of tropical intraseasonal convective anomalies. *J. Clim.* **2004**, *17*, 2078–2095. [[CrossRef](#)]
49. Rummukainen, M.; Räisänen, J.; Bringfelt, B.; Ullerstig, A.; Omstedt, A.; Willén, U.; Hansson, U.; Jones, C. A regional climate model for northern Europe: Model description and results from the downscaling of two GCM control simulations. *Clim. Dyn.* **2001**, *17*, 339–359. [[CrossRef](#)]
50. Pope, V.D.; Gallani, M.L.; Rowntree, P.R.; Stratton, R.A. The impact of new physical parametrizations in the Hadley Centre climate model: HadAM3. *Clim. Dyn.* **2000**, *16*, 123–146. [[CrossRef](#)]
51. Nakićenović, N. *Intergovernmental Panel on Climate Change. Working Group III*; Cambridge University Press: Cambridge, UK, 2000.
52. Rayner, N.A. Global analyses of sea surface temperature, sea ice, and night marine air temperature since the late nineteenth century. *J. Geophys. Res.* **2003**, *108*, 4407. [[CrossRef](#)]
53. Rowell, D.P. A scenario of European climate change for the late twenty-first century: Seasonal means and interannual variability. *Clim. Dyn.* **2005**, *25*, 837–849. [[CrossRef](#)]
54. Christensen, J.H.; Carter, T.R.; Rummukainen, M.; Amanatidis, G. Evaluating the performance and utility of regional climate models: The PRUDENCE project. *Clim. Chang.* **2007**, *81*, 1–6. [[CrossRef](#)]
55. Gu, G.; Adler, R.F.; Huffman, G.J. Long-term changes/trends in surface temperature and precipitation during the satellite era (1979–2012). *Clim. Dyn.* **2016**, *46*, 1091–1105. [[CrossRef](#)]

56. Tapiador, F.J.; Navarro, A.; Jiménez, A.; Moreno, R.; García-Ortega, E. Discrepancies with Satellite Observations in the Spatial Structure of Global Precipitation as Derived from Global Climate Models. *Q. J. R. Meteorol. Soc.* **2018**. [[CrossRef](#)]
57. Knist, S.; Goergen, K.; Buonomo, E.; Christensen, O.B.; Colette, A.; Cardoso, R.M.; Fealy, R.; Fernández, J.; García-Díez, M.; Jacob, D.; et al. Land-atmosphere coupling in EURO-CORDEX evaluation experiments. *J. Geophys. Res. Atmos.* **2017**, *122*, 79–103. [[CrossRef](#)]
58. Mascaro, G.; Viola, F.; Deidda, R. Evaluation of Precipitation From EURO-CORDEX Regional Climate Simulations in a Small-Scale Mediterranean Site. *J. Geophys. Res. Atmos.* **2018**, *123*, 1604–1625. [[CrossRef](#)]
59. Hosseinzadehtalaei, P.; Tabari, H.; Willems, P. Precipitation intensity-duration-frequency curves for central Belgium with an ensemble of EURO-CORDEX simulations, and associated uncertainties. *Atmos. Res.* **2018**, *200*, 1–12. [[CrossRef](#)]
60. Cardoso, R.M.; Soares, P.M.M.; Lima, D.C.A.; Semedo, A. The impact of climate change on the Iberian low-level wind jet: EURO-CORDEX regional climate simulation. *Tellus A Dyn. Meteorol. Oceanogr.* **2018**, *68*. [[CrossRef](#)]
61. Smiatek, G.; Kunstmann, H.; Senatore, A. EURO-CORDEX regional climate model analysis for the Greater Alpine Region: Performance and expected future change. *J. Geophys. Res. Atmos.* **2016**, *121*, 7710–7728. [[CrossRef](#)]
62. Dosio, A. Projections of climate change indices of temperature and precipitation from an ensemble of bias-adjusted high-resolution EURO-CORDEX regional climate models. *J. Geophys. Res. Atmos.* **2016**, *121*, 5488–5511. [[CrossRef](#)]
63. Dalelane, C.; Früh, B.; Steger, C.; Walter, A. A pragmatic approach to build a reduced regional climate projection ensemble for Germany using the EURO-CORDEX 8.5 ensemble. *J. Appl. Meteorol. Climatol.* **2018**, *57*, 477–491. [[CrossRef](#)]
64. Jacob, D.; Petersen, J.; Eggert, B.; Alias, A.; Christensen, O.B.; Bouwer, L.M.; Braun, A.; Colette, A.; Déqué, M.; Georgievski, G.; et al. EURO-CORDEX: New high-resolution climate change projections for European impact research. *Reg. Environ. Chang.* **2014**, *14*, 563–578. [[CrossRef](#)]



© 2018 by the authors. Licensee MDPI, Basel, Switzerland. This article is an open access article distributed under the terms and conditions of the Creative Commons Attribution (CC BY) license (<http://creativecommons.org/licenses/by/4.0/>).